Acta Crystallographica Section F
Structural Biology and Crystallization Communications
ISSN 1744-3091

Crystallization and preliminary X-ray diffraction analysis of diaminopimelate epimerase from *Escherichia coli*

Lilian Hor,[a,b,c]‡ Renwick C. J. Dobson,[b,c,d]‡ Con Dogovski,[b,c] Craig A. Hutton[a,c] and Matthew A. Perugini[b,c]*

[a]School of Chemistry, The University of Melbourne, Parkville, Victoria 3010, Australia, [b]Department of Biochemistry and Molecular Biology, The University of Melbourne, Parkville, Victoria 3010, Australia, [c]Bio21 Molecular Science and Biotechnology Institute, 30 Flemington Road, The University of Melbourne, Parkville, Victoria 3010, Australia, and [d]School of Biological Sciences, University of Canterbury, Private Bag 4800, Christchurch, New Zealand

‡ These authors contributed equally to this work.

Correspondence e-mail: perugini@unimelb.edu.au

Received 31 August 2009
Accepted 11 November 2009

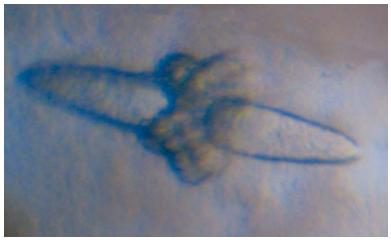

Diaminopimelate (DAP) epimerase (EC 5.1.1.7) catalyzes the penultimate step of lysine biosynthesis in bacteria and plants, converting L,L-diaminopimelate to *meso*-diaminopimelate. Here, the cloning, expression, purification, crystallization and preliminary X-ray diffraction analysis of DAP epimerase from *Escherichia coli* are presented. Crystals were obtained in space group $P4_12_12$ and diffracted to 2.0 Å resolution, with unit-cell parameters $a = b = 89.4$, $c = 179.6$ Å. Molecular replacement was conducted using *Bacillus anthracis* DAP epimerase as a search model and showed the presence of two molecules in the asymmetric unit, with an initial R_{free} of 0.456 and R_{work} of 0.416.

1. Introduction

Diaminopimelate (DAP) epimerase (EC 5.1.1.7) is a member of the PLP-independent amino-acid racemases. It catalyzes the stereoinversion of L,L-diaminopimelate to *meso*-diaminopimelate in the lysine-biosynthetic pathway in plants and bacteria. Since lysine biosynthesis does not occur in animals, the members of the pathway, such as DAP epimerase, are attractive targets for rational antibiotic design (Hutton *et al.*, 2003, 2007).

The catalytic mechanism of DAP epimerase has been extensively studied, showing that the enzyme utilizes a 'two-base' mechanism involving a pair of cysteine residues (Pillai *et al.*, 2006; Wiseman & Nichols, 1984). One residue acts as a base and the other as an acid, resulting in an inversion of stereochemical configuration.

The structures of DAP epimerases from a variety of organisms have been determined, including those from *Haemophilus influenzae* (Cirilli *et al.*, 1998; Lloyd *et al.*, 2004), *Mycobacterium tuberculosis* (Usha *et al.*, 2009) and the plant *Arabidopsis thaliana* (Pillai *et al.*, 2009). All of the structures show a two-domain α/β-fold, with each domain contributing one active-site cysteine. The enzyme is a symmetrical monomer comprised of two domains, each containing eight β-strands and two α-helices. This unique fold was first observed in *H. influenzae* DAP epimerase; since then, a number of proteins including a phenazine-biosynthetic protein (Blankenfeldt *et al.*, 2004; Parsons *et al.*, 2004), a proline racemase (Buschiazzo *et al.*, 2006) and a methylaconitate isomerase (Garvey *et al.*, 2007) have also been shown to adopt this fold.

Here, we present the cloning, recombinant expression, purification, crystallization and preliminary crystallographic studies of DAP epimerase from *Escherichia coli*.

2. Materials and methods

2.1. Cloning, expression and purification of *E. coli* DAP epimerase

The *dapF* gene encoding DAP epimerase, including flanking sequences, was amplified by PCR from *E. coli* genomic DNA using primers 5′-GTCCATCCCAGGTGAATTAC-3′ and 5′-GTGAGTG-TTTCCTGCAGTTC-3′. The PCR product was subsequently cloned into pCR-Blunt II-TOPO (Invitrogen) using the Zero Blunt TOPO PCR Cloning Kit (Invitrogen). *Nde*I and *Bam*HI restriction sites

were incorporated into the 5′ and 3′ ends of the *dapF* gene by PCR using the primers 5′-CATATGCAGTTCTCGAAAATGC-3′ and 5′-GGATCCTCAATGGTGATGGTGATGGTGTAGATGAATAAA-TCCGTCGT-3′, respectively. The 3′-end primer was also designed to append a carboxy-terminal hexahistidine tag to the *dapF* open reading frame. The resulting PCR product was digested with the restriction enzymes *Nde*I and *Bam*HI and subsequently cloned into the corresponding sites of the pET11a expression vector (New England Biolabs). The identity of the *E. coli dapF* gene was verified by restriction analysis and dideoxynucleotide sequencing.

E. coli DAP epimerase was expressed in *E. coli* BL21 (DE3) harbouring the pET11a-*dapF* plasmid by culturing at 293 K in auto-induction media (Studier, 2005) containing 100 µg ml^{-1} ampicillin for 25 h. The cells were harvested by centrifugation at 5000*g* for 15 min at 277 K and the cell pellet was stored at 253 K. Cell lysates were prepared as described elsewhere (Burgess *et al.*, 2008; Dobson *et al.*, 2008; Voss *et al.*, 2009). Briefly, harvested cells were resuspended in 20 m*M* Tris, 500 m*M* NaCl, 20 m*M* imidazole, 5 m*M* DTT pH 8.0 and lysed by sonication and the supernatant was collected by centrifugation at 30 000*g* for 20 min at 277 K. DAP epimerase was then purified at 277 K from the cell lysate by immobilized metal-affinity chromatography using 3 × 5 ml HisTrap HP columns connected in series (GE Healthcare) pre-equilibrated with 20 m*M* Tris, 500 m*M* NaCl, 20 m*M* imidazole, 1 m*M* DTT pH 8.0. His-tagged DAP epimerase was then eluted with a 20–500 m*M* imidazole gradient over six column volumes. Fractions were subsequently analysed by SDS–PAGE and those containing pure DAP epimerase were pooled and dialyzed into 20 m*M* Tris, 1 m*M* DTT pH 7.8. The enzyme was then concentrated to 12 mg ml^{-1} and further purified by gel-filtration chromatography using a 1.0 cm (diameter) × 30 cm (length) Sephacryl S-200 column (GE Healthcare) pre-equilibrated in 20 m*M* Tris, 1 m*M* DTT pH 7.8. For crystallization trials, the recombinant protein was concentrated to 8.0 mg ml^{-1}.

2.2. Crystallization of *E. coli* DAP epimerase

Crystallization screens were conducted as described previously (Atkinson *et al.*, 2009; Burgess *et al.*, 2008; Dobson *et al.*, 2008; Voss *et al.*, 2009). Initial protein-crystallization experiments were performed at the CSIRO node of the Bio21 Collaborative Crystallization Centre (C3) using the PACT Suite and JCSG+ Suite crystal screens at 281 and 293 K (Newman *et al.*, 2005, 2008). The screens were set up using the sitting-drop vapour-diffusion method with droplets consisting of 150 nl protein solution and 150 nl reservoir solution. Conditions that yielded crystals were replicated using the hanging-drop vapour-diffusion method with drops containing 2 µl protein solution and 2 µl precipitant solution at 281 and 293 K. These conditions were also trialled with the addition of 5 m*M* TCEP. The addition of TCEP yielded crystals with different morphologies to those obtained with DTT alone. The crystal shown in Fig. 1 was obtained at 293 K from a 4 µl drop formed from 2 µl protein solution (8.0 mg ml^{-1} in 20 m*M* Tris, 5 m*M* DTT, 5 m*M* TCEP pH 7.8) and 2 µl precipitant [200 m*M* sodium nitrate, 20%(*w*/*v*) polyethylene glycol 3350, 100 m*M* bis-tris propane pH 8.5]. We noted that only freshly purified protein readily produced crystals.

2.3. Data collection and processing

For X-ray data collection, the crystal was soaked in a cryoprotectant solution consisting of reservoir solution made up with 20%(*v*/*v*) glycerol and directly flash-cooled in liquid nitrogen. Intensity data were collected at 110 K at the Australian Synchrotron (MX2 beamline). Data were collected in 0.5° oscillations over 95° using an ADSC Q315r image-plate detector positioned 230 mm from the crystal, with an exposure time of 0.5 s and 95% attenuation. The diffraction data were processed using the programs *MOSFLM* (Leslie, 1991) and *SCALA* (Collaborative Computational Project, Number 4, 1994). Although 90° of data were initially collected, the resolution and quality of the diffraction data decreased (as judged by an increased batch $R_{\rm merge}$ and number of rejected reflections); as such, the final 34° wedge of data was omitted from subsequent steps.

3. Results and discussion

E. coli DAP epimerase was cloned, expressed and purified to homogeneity by a two-step purification protocol involving Ni^{2+}-affinity chromatography and gel-filtration chromatography. Fractions following each step of the purification strategy were assessed by SDS–PAGE (Fig. 2) and the enzyme activity was measured using the DAP epimerase–DAP dehydrogenase coupled assay (Cox *et al.*,

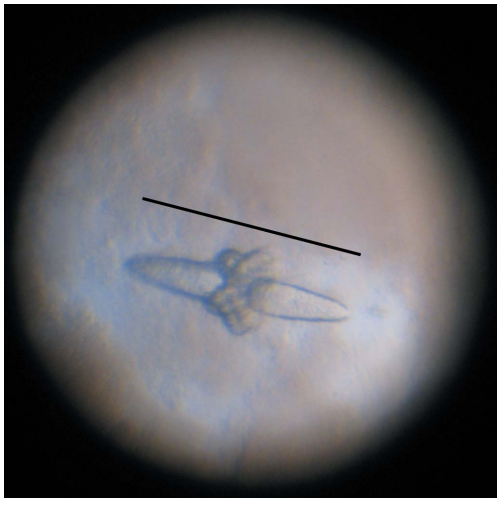

Figure 1
Crystal of *E. coli* DAP epimerase. The bar represents 150 µm.

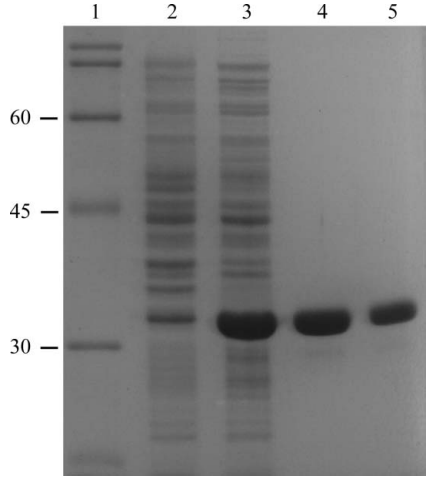

Figure 2
SDS–PAGE analysis of *E. coli* DAP epimerase (molecular mass 31 031.56 Da) at each stage of the purification. Lane 1, molecular-mass markers (kDa); lane 2, cell lysate pre-induction; lane 3, cell lysate post-induction; lane 4, after Ni^{2+}-affinity liquid chromatography; lane 5, after gel-filtration liquid chromatography. The SDS–PAGE gel (12%) was stained with Coomassie Brilliant Blue R250.

Table 1
Purification of *E. coli* DAP epimerase.

One unit of enzyme activity is equal to the reduction of 1 µmol of $NADP^+$ per second.

	Total protein (mg)	Total activity (U)	Specific activity (U mg^{-1})	Degree of purification (fold)
Crude extract	504	103	0.205	
Ni^{2+}-affinity liquid chromatography	98.7	56.7	0.574	2.80
Gel-filtration chromatography	39.2	46.1	1.18	5.76

2002). Gel-filtration chromatographic analysis indicated evidence of large-molecular-mass species that were believed to be aggregated recombinant DAP epimerase. The aggregate did not display enzymatic activity. Removal of this incompetent enzyme resulted in a twofold increase in the specific activity (Table 1).

E. coli DAP epimerase was found to crystallize in a number of conditions from the PACT screen, in particular those containing PEG 3350 and bis-tris propane buffer. The crystal in Fig. 1 appeared after 2 d and continued to grow to a length of 150 µm in the longest dimension over a further 5 d.

Data were collected at the Australian Synchrotron (Melbourne, Australia) using the micro-focus beamline MX2. This allowed only one end of the crystal to be exposed to X-rays in order to prevent diffraction from the cluster of crystals that can be observed in the midsection of the main crystal in Fig. 1. The crystal showed excellent diffraction (to beyond 2.0 Å resolution; Fig. 3) and belonged to space group $P4_12_12$, with unit-cell parameters $a = b = 89.4$, $c = 179.6$ Å. $R_{\rm merge}$ was 0.077, $R_{\rm p.i.m.}$ was 0.039, $R_{\rm r.i.m}$ was 0.087, $V_{\rm M}$ was 2.89 Å^3 Da^{-1} and the estimated solvent content was 57% assuming the presence of two molecules in the asymmetric unit. Complete data-collection statistics are summarized in Table 2.

Molecular replacement using DAP epimerase from *Bacillus anthracis* as a search model (PDB code 2otn; 37% sequence identity) was performed using *Phaser* (McCoy *et al.*, 2007). This confirmed the presence of two molecules in the asymmetric unit, with an initial $R_{\rm free}$ of 0.456 and $R_{\rm work}$ of 0.416. Further model building and refinement continues.

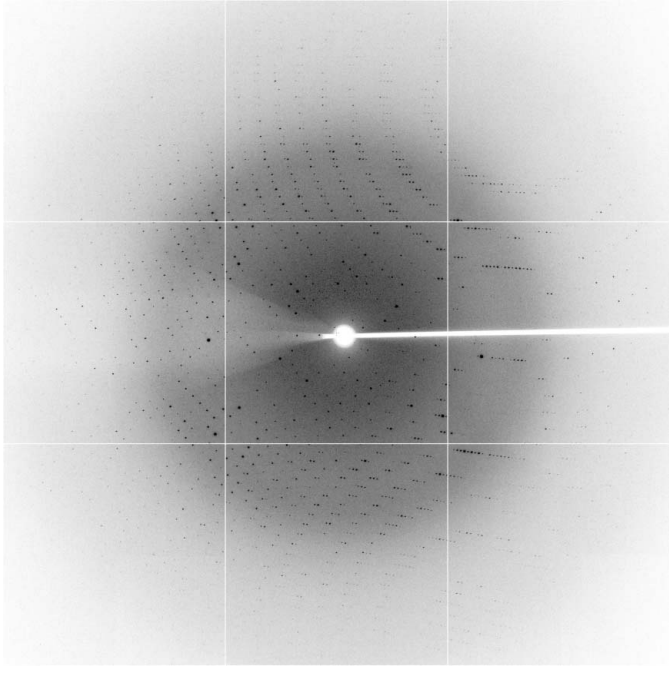

Figure 3
An X-ray diffraction frame of the cryocooled crystal of *E. coli* DAP epimerase. The crystal diffracted to beyond 2.0 Å (corners).

Table 2
X-ray data-collection statistics.

Values in parentheses are for the highest resolution shell. The Matthews coefficient and solvent content are based on two monomers of molecular weight 31 031.56 Da in the asymmetric unit (ASU).

Wavelength (Å)	0.97946
No. of images	111
Oscillation (°)	0.5
Space group	$P4_12_12$
Unit-cell parameters (Å)	$a = b = 89.4$, $c = 179.6$
Resolution (Å)	44.69–2.00 (2.11–2.00)
Observed reflections	215760 (29012)
Unique reflections	47663 (6683)
Completeness (%)	96.1 (93.7)
$R_{\rm merge}$†	0.077 (0.339)
$R_{\rm p.i.m.}$‡	0.039 (0.137)
$R_{\rm r.i.m.}$	0.087 (0.385)
Mean $I/\sigma(I)$	13.0 (4.2)
Redundancy	4.5 (4.3)
Wilson B value (Å^2)	23.4
Molecules per ASU	2
$V_{\rm M}$ (Å^3 Da^{-1})	2.89
Solvent content (%)	57

† $R_{\rm merge} = \sum_{hkl}\sum_i |I_i(hkl) - \langle I(hkl)\rangle| / \sum_{hkl}\sum_i I_i(hkl)$. ‡ $R_{\rm p.i.m.} = \sum_{hkl}[1/(N-1)]^{1/2} \times \sum_i |I_i(hkl) - \langle I(hkl)\rangle| / \sum_{hkl}\sum_i I_i(hkl)$.

We would firstly like to acknowledge the support and assistance of the friendly staff, especially Dr Janet Newman, at the Bio21 Collaborative Crystallographic Centre at CSIRO Molecular and Health Technologies, Parkville, Melbourne as well as all members of the Perugini and Hutton laboratories for helpful discussions during the preparation of this manuscript. This research was undertaken on the MX2 beamline at the Australian Synchrotron, Victoria, Australia. The views expressed herein are those of the authors and are not necessarily those of the owner or operator of the Australian Synchrotron. Finally, we acknowledge the Defense Threat Reduction Agency (DTRA; Project ID AB07CBT004) for program funding, the Australian Research Council for providing a Future Fellowship to MAP and The University of Melbourne for the C. R. Roper Research Fellowhip to RCJD.

References

Atkinson, S. C., Dobson, R. C. J., Newman, J. M., Gorman, M. A., Dogovski, C., Parker, M. W. & Perugini, M. A. (2009). *Acta Cryst.* F**65**, 253–255.
Blankenfeldt, W., Kuzin, A. P., Skarina, T., Korniyenko, Y., Tong, L., Bayer, P., Janning, P., Thomashow, L. S. & Mavrodi, D. V. (2004). *Proc. Natl Acad. Sci. USA*, **101**, 16431–16436.
Burgess, B. R., Dobson, R. C. J., Dogovski, C., Jameson, G. B., Parker, M. W. & Perugini, M. A. (2008). *Acta Cryst.* F**64**, 659–661.
Buschiazzo, A., Goytia, M., Schaeffer, F., Degrave, W., Shepard, W., Gregoire, C., Chamond, N., Cosson, A., Berneman, A., Coatnoan, N., Alzari, P. M. & Minoprio, P. (2006). *Proc. Natl Acad. Sci. USA*, **103**, 1705–1710.
Cirilli, M., Zheng, R., Scapin, G. & Blanchard, J. S. (1998). *Biochemistry*, **37**, 16452–16458.
Collaborative Computational Project, Number 4 (1994). *Acta Cryst.* D**50**, 760–763.
Cox, R. J., Durston, J. & Roper, D. I. (2002). *J. Chem. Soc. Perkin Trans.* **1**, 1029–1035.
Dobson, R. C. J., Atkinson, S. C., Gorman, M. A., Newman, J. M., Parker, M. W. & Perugini, M. A. (2008). *Acta Cryst.* F**64**, 206–208.
Garvey, G. S., Rocco, C. J., Escalante-Semerena, J. C. & Rayment, I. (2007). *Protein Sci.* **16**, 1274–1284.
Hutton, C. A., Perugini, M. A. & Gerrard, J. A. (2007). *Mol. Biosyst.* **3**, 458–465.

Hutton, C. A., Southwood, T. J. & Turner, J. J. (2003). *Mini Rev. Med. Chem.* **3**, 115–127.
Leslie, A. G. W. (1991). *Crystallographic Computing 5: From Chemistry to Biology*, edited by D. Moras, A. D. Podjarny & J. C. Thierry, pp. 50–61. Oxford University Press.
Lloyd, A. J., Huyton, T., Turkenburg, J. & Roper, D. I. (2004). *Acta Cryst.* D**60**, 397–400.
McCoy, A. J., Grosse-Kunstleve, R. W., Adams, P. D., Winn, M. D., Storoni, L. C. & Read, R. J. (2007). *J. Appl. Cryst.* **40**, 658–674.
Newman, J., Egan, D., Walter, T. S., Meged, R., Berry, I., Ben Jelloul, M., Sussman, J. L., Stuart, D. I. & Perrakis, A. (2005). *Acta Cryst.* D**61**, 1426–1431.
Newman, J., Pham, T. M. & Peat, T. S. (2008). *Acta Cryst.* F**64**, 991–996.
Parsons, J. F., Song, F., Parsons, L., Calabrese, K., Eisenstein, E. & Ladner, J. E. (2004). *Biochemistry*, **43**, 12427–12435.
Pillai, B., Cherney, M. M., Diaper, C. M., Sutherland, A., Blanchard, J. S., Vederas, J. C. & James, M. N. G. (2006). *Proc. Natl Acad. Sci. USA*, **103**, 8668–8673.
Pillai, B., Moorthie, V. A., van Belkum, M. J., Marcus, S. L., Cherney, M. M., Diaper, C. M., Vederas, J. C. & James, M. N. G. (2009). *J. Mol. Biol.* **385**, 580–594.
Studier, F. W. (2005). *Protein Expr. Purif.* **42**, 207–234.
Usha, V., Dover, L. G., Roper, D. I., Fütterer, K. & Besra, G. S. (2009). *Acta Cryst.* D**65**, 383–387.
Voss, J. E., Scally, S. W., Taylor, N. L., Dogovski, C., Alderton, M. R., Hutton, C. A., Gerrard, J. A., Parker, M. W., Dobson, R. C. J. & Perugini, M. A. (2009). *Acta Cryst.* F**65**, 188–191.
Wiseman, J. S. & Nichols, J. S. (1984). *J. Biol. Chem.* **259**, 8907–8914.